EPJ Web of Conferences **350**, 01003 (2026) https://doi.org/10.1051/epjconf/202635001003
ICASIN'2025

Neutronic and thermal-hydraulic performance analysis of a novel thorium-based fuel in dual-cooled annular assemblies for SMR applications

Hanan Rifai[1], *Ouadie kabach*[2*], *Sinem Uzun*[3], *Yasin Genç*[4], *Bedrettin Uzun*[5], *Hamid Amsil*[6], *El Mahjoub Chakir*[2] *and Zouhair Sadoune*[1]

[1]LESIPME, Faculty of Sciences, Ibn Tofail University, Kenitra, Morocco.
[2]LPMS, Faculty of Sciences, Ibn Tofail University, Kenitra, Morocco.
[3]Faculty of Engineering and Architecture, Erzincan Binali Yıldırım University, Erzincan, Türkiye
[4]Ministry of Interior, Disaster and Emergency Management Presidency, Ankara, Türkiye
[5]Republic of Turkey Northeast Anatolia Development Agency, Erzincan, Türkiye
[6]National Center for Energy, Sciences and Nuclear Technique, Rabat, Morocco

Abstract. A coupled neutronic and thermal-hydraulic assessment is performed for a dual-cooled annular fuel concept applied to light-water SMR conditions. A mixed thorium-based oxide, $(Th\text{-}^{233}U\text{-}^{235}U)O_2$, is evaluated against conventional UO_2 and solid-pin benchmarks while sweeping the inner moderator radius (0.05-0.43165 cm) at constant fuel volume. The thorium annular cases sustain an infinite multiplication factor (k_{inf}) of 1.002-1.003 at EOC and achieve 3-batch discharge burnups of 166.3-173.5 GWd/t, compared with 142.4 GWd/t for solid UO_2. Radial peaking remains low (maximum PPF ≈ 1.056, well below the 1.65 Westinghouse-types PWR design limit). All configurations exhibit negative FTC and MTC, with stronger negative feedback at larger inner radii. Thermal-hydraulic results show smooth coolant heating and robust DNBR margins (minimum ~ 2.3) with negligible sensitivity to inner radius. These outcomes support the feasibility of thorium-based annular fuel for SMR deployment with improved fuel utilization and preserved safety margins.

Keywords: Thorium fuel, Annular fuel, SMR, Neutronic–thermal coupling, Burnup

1 Introduction

Conventional LWR-based SMRs typically rely on solid UO_2 pellets in Zircaloy-clad rods arranged in a square lattice. To improve thermal margins and safety, alternative geometries have been proposed, among which the dual-cooled annular fuel is particularly attractive. This concept employs a hollow cylindrical fuel ring cooled on both the inner and outer surfaces, which shortens the conduction path and increases heat-transfer area, thereby enhancing heat removal and DNBR margins. Kazimi et al. showed that the larger wetted

* Corresponding author: ouadie.kabach10@gmail.com

perimeter reduces heat flux on both heated surfaces and can enable substantial power-density increases while maintaining lower peak fuel temperatures than solid rods [1–4]. Annular concepts have been pursued for full-scale PWRs (e.g., KAERI's OPR-1000 studies) and also evaluated for SMRs such as NuScale, demonstrating broad applicability across reactor sizes [5–9]. Beyond geometry, fuel composition strongly affects safety feedback and fuel utilization. Building on our earlier work, we consider the mixed oxide $(Th\text{-}^{233}U\text{-}^{235}U)O_2$ as an alternative to conventional UO_2 and to thorium fuels such as $(Th\text{-}^{235}U)O_2$ and $(Th\text{-}^{233}U)O_2$ [10–12]. This formulation combines fertile ^{232}Th with two fissile contributors, ^{233}U and ^{235}U, leveraging their complementary neutronic behavior. Prior assessments indicate that this fuel can provide a more negative fuel temperature coefficient (FTC) and moderator temperature coefficient (MTC) relative to $(Th\text{-}^{233}U)O_2$, and improved fissile economy [10,11]. The objective of the present work is to perform coupled neutronic and thermal-hydraulic analyses of fuel channels while quantifying the impact of the inner moderator radius in dual-cooled annular pins, a design parameter known to influence moderation efficiency and, consequently, performance. All configurations are evaluated in the AP300™ SMR context, used here as the reference core. Neutronic outcomes include the FTC and MTC, discharge burnup, and power peaking factors (PPF). The thermal-hydraulic assessment focuses on fuel temperature behavior and the DNBR.

2 Model design and input parameters

2.1 Description of the benchmark assembly used for the investigation

In this work, the Westinghouse AP300™ small modular reactor assembly is adopted as the reference for the benchmark calculations. AP300 is a Generation III+ pressurized water reactor concept developed to deliver 330 MWe from a thermal output of 990 MWt. The core layout comprises 121 fuel assemblies arranged in a 17 × 17 square-lattice configuration. The assemblies employ UO_2 fuel with ^{235}U enrichment below 5 wt.%, consistent with standard commercial PWR fuel specifications. The key technical characteristics of the selected SMR model are summarized in Table 1[13,14].

Table 1. Technical parameters of the considered SMR model [13].

Parameter	Specification
Primary system circulation	Forced circulation; two reactor coolant pumps
Core coolant temperature (°C), inlet/outlet	302 / 325
Refueling interval (months)	36 (extendable up to 48)
Reactivity control means	Control rods and soluble boron
Safety system concept	Passive safety features (AP1000-derived)
Design lifetime (years)	80

2.2 Specification of the proposed assembly and models

LW-SMRs can exhibit thermal-hydraulic responses and neutron flux distributions that differ from large LWRs because of their compact cores, motivating a reassessment of fuel-element geometry and operating constraints. While solid cylindrical pellets are proven in commercial reactors, advanced concepts may be limited by strong centerline heating and steep radial temperature gradients, which can restrict achievable power density and uprating potential [2,5]. To address these constraints, an internally and externally cooled annular fuel pin provides two heat-transfer surfaces, reducing the effective conduction path and increasing the fuel-coolant heat-transfer area, thereby lowering peak fuel temperatures. This work evaluates thorium-based $(Th\text{-}^{233}U\text{-}^{235}U)O_2$ against the solid UO_2 reference and quantifies the effect of inner channel size on coupled neutronic and thermal-hydraulic behavior. A parametric sweep of the inner moderator radius is performed from 0.05 to 0.43165 cm, consistent with the optimization guidance of Kazimi and Hejzlar [1]. For consistent comparison, the fuel volume is kept constant across cases, and the gap and cladding thicknesses are fixed at 0.0082 cm and 0.0572 cm, respectively, isolating the impact of inner moderator radius variation. Figure 1 presents the DRAGON lattice models; Tables 2-4 summarize fuel properties, assembly parameters, and case identifiers, respectively. Figure 1. DRAGON models of the solid and dual-cooled annular assemblies and associated pin-cell geometries.

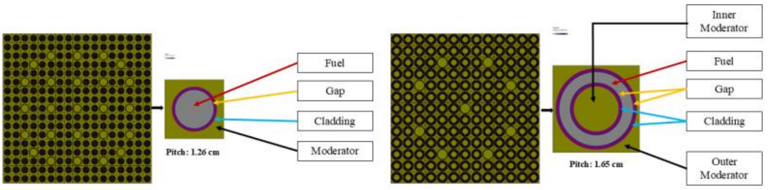

Fig. 1. Computational modeling of solid and dual-cooled annular assembly configurations and fuel elements via DRAGON code**.**

Table 2. Properties of the analyzed fuel type [11].

Fuel	Density (g/cm^3)	Fissile enrichment (wt.%)
UO_2	10.41	4.95 % (U-235)
(Th-^{233}U-^{235}U)O_2	9.50	2.475 % (U-233) + 2.475 % (U-235)

Table 3. Assembly-level parameters considered in the simulations.

Parameter	**Solid**	**Annular**
Rod array	17 × 17	13 × 13
Fuel rods (count)	264	160
Guide tubes (count)	24	9
Assembly pitch (cm)	21.5	21.5
Rod lattice pitch (cm)	1.26	1.65
Fuel outer radius (cm)	0.40960	0.51509 / 0.52854 / 0.54626 / 0.56784 / 0.62090 / 0.68454 / 0.70644
Outer gap outer radius (cm)	0.41780	0.52329 / 0.53674 / 0.55446 / 0.57604 / 0.62910 / 0.69274 / 0.71464
Outer cladding outer radius (cm)	0.47500	0.58049 / 0.59394 / 0.61166 / 0.63324 / 0.68630 / 0.74994 / 0.77184
Inner cladding inner radius (cm)	-	0.05 / 0.10 / 0.15 / 0.20 / 0.30 / 0.40 / 0.43165
Inner cladding outer radius (cm)	-	0.10720 / 0.15720 / 0.20720 / 0.25720 / 0.35720 / 0.45720 / 0.48885
Inner gap outer radius (cm)	-	0.11540 / 0.16540 / 0.21540 / 0.26540 / 0.36540 / 0.46540 / 0.49705
Guide tube inner radius (cm)	0.56	0.71
Guide tube outer radius (cm)	0.60	0.77

Table 4. Description of the assembly cases investigated in the study with corresponding IDs**.**

Case ID	Description	Case ID	Description
So_UO_2	Solid with UO_2 fuel	DC_(Th-^{233}U-^{235}U)O_2_case4	Inner moderator radius is 2.0 mm
So_(Th-^{233}U-^{235}U)O_2	Solid with (Th-^{233}U-^{235}U)O_2 fuel	DC_(Th-^{233}U-^{235}U)O_2_case5	Inner moderator radius is 3.0 mm
DC_(Th-^{233}U-^{235}U)O_2_case1	Inner moderator radius is 0.5 mm	DC_(Th-^{233}U-^{235}U)O_2_case6	Inner moderator radius is 4.0 mm
DC_(Th-^{233}U-^{235}U)O_2_case2	Inner moderator radius is 1.0 mm	DC_(Th-^{233}U-^{235}U)O_2_case7	Inner moderator radius is 4.3165 mm
DC_(Th-^{233}U-^{235}U)O_2_case3	Inner moderator radius is 1.5 mm	DC_(Th-^{233}U-^{235}U)O_2_case4	Inner moderator radius is 2.0 mm

2.3 Calculation procedures for neutronic analysis

All lattice calculations were performed with the DRAGON reactor-physics code, developed at Polytechnique Montréal for neutron transport analyses in unit cells and fuel assemblies [15]. In this work, DRAGON simulations were used to extract the neutronic quantities required for the coupled assessment, including flux distributions, radial power peaking factors, temperature reactivity coefficients, and burnup-dependent isotopic evolution. At the modeling level, individual pin cells were represented using mixed Cartesian and annular geometrical descriptions within assembly calculations. Control-rod guide locations were modeled as water-filled regions (without soluble boron) to simplify the lattice representation. The DRAGON workflow relied on standard modules: geometry definition (GEO), spatial tracking (EXCELT), transport solution with MCCGT (Suslov long-characteristics), and self-shielding treatment (SHI). Nuclear data were taken from ENDF/B-VIII.0 in draglib format with the SHEM-361 group structure. The ASM and FLU modules were used for collision-probability/flux calculations, while burnup and post-processing were carried out with EVO and EDI (homogenization and condensation), respectively [16]. Fuel discharge burnup was estimated using the Linear Reactivity Model (LRM), which is commonly applied to PWRs because the initial reactivity versus burnup is approximately linear [17]. Reactivity is written as:

$$\rho = \frac{K_{inf} - (1 + L)}{K_{inf}} \tag{1}$$

k_{inf} is the infinite-lattice multiplication factor, and L is the fractional neutron leakage. To account for enhanced leakage in compact SMR cores, a 7% leakage penalty was adopted (higher than the ~3% typically assumed for large PWRs), consistent with SMR literature [18,19]. Accordingly, single-batch discharge burnup was defined at kinf=1. 07. For an N_{NB}-batch management scheme, the corresponding discharge burnup (reported in GWd/t) was obtained from:

$$B_{Discharge} = \frac{2N_{NB}}{(N_{NB} + 1)} B_{SB} \tag{2}$$

where B_{SB} is the single-batch discharge burnup, and N_{NB} is the number of batches in the shuffling strategy (e.g., a three-batch scheme increases discharge burnup by a factor of 1.5 relative to single-batch operation). Reactivity feedbacks were evaluated through the FTC and MTC, which quantify the neutronic response to thermal perturbations. The FTC was determined by perturbing fuel temperature and computing:

$$FTC = \frac{K_{inf}(T) - K_{inf,0}}{K_{inf,0}\Delta T} \tag{3}$$

The MTC was computed by applying simultaneous moderator temperature and density changes:

$$MTC = \frac{K_{inf}(T, \rho) - K_{inf,0}}{K_{inf,0}\Delta T} \tag{4}$$

2.4 Calculation procedures for thermal-hydraulic analysis

Neutronic calculations were first performed with MCNP to solve the neutron transport problem and generate the three-dimensional power (heat source) distribution in the assembly. These results were then used to identify the limiting (hot) channel selected for the thermal-hydraulic evaluation. The obtained power shapes were extracted and reformatted as inputs for a representative single-channel thermal-hydraulic model covering both solid and annular fuel geometries (Fig. 3). The fuel, cladding, and coolant were treated as distinct domains. Heat generation was assumed volumetric within the fuel, conducted radially through the cladding, and removed at the cladding–coolant interface by convection.

Thermophysical properties (e.g., conductivity, heat capacity, and density) were treated as temperature-dependent. Using conservative assumptions, this hot-channel approach provided the key thermal metrics required for comparison, including peak fuel temperature, pressure drop, heat flux, and DNBR [20–22]. The coolant region was discretized following subchannel-analysis practice to solve the steady, single-phase conservation equations for mass, momentum, and energy. Hydraulic losses were evaluated with standard correlations, and single-phase convective heat transfer coefficients were estimated using the Dittus-Boelter relation. Importantly, Dittus-Boelter was used only for single-phase convection; critical heat flux and DNB margins were evaluated with the W-3 CHF correlation, which is accepted for PWR applications and has been benchmarked against extensive bundle test databases [22–24]. The model is governed by the continuity, energy, and momentum equations:

$$\frac{\partial \rho}{\partial t} + \nabla \cdot (\rho \vec{v}) = 0 \tag{5}$$

$$\frac{\partial(\rho h)}{\partial t} + \nabla \cdot (\rho h \vec{v}) = -\nabla \vec{q} + \dot{q} + \frac{\partial(p)}{\partial t} + \nabla.(p\vec{v}) + \tau \tag{6}$$

$$\frac{\partial(\rho \vec{v})}{\partial t} + \nabla \cdot (\rho \vec{v}\vec{v}) = \nabla.p + \nabla\tau + \rho\vec{g} \tag{7}$$

where ρ is coolant density, $\vec{v}$ is velocity, his specific enthalpy, $\vec{q}$ is the heat-flux vector, $\dot{q}$ is the volumetric heat source, p is pressure, τ is the viscous stress tensor, and $\vec{g}$ is gravitational acceleration.

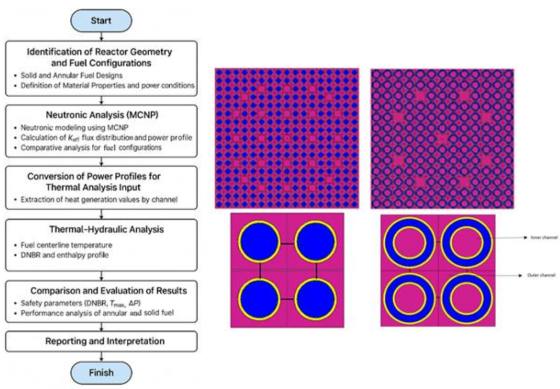

Fig. 2. Integrated neutronic and thermal-hydraulic workflow for fuel performance assessment.

3 Results and discussion

3.1 Neutronic results

In neutronics, k_{inf} quantifies lattice criticality as the ratio of neutrons produced by fission to neutrons lost by absorption; larger k_{inf} implies a stronger ability to sustain the chain reaction. Accounting for SMR leakage with a 7% penalty, the critical threshold is set to k_{inf} =1.07. Figure 3 shows that k_{inf} decreases with burnup for all cases, with an initially steeper drop attributed to the rapid buildup of strong absorbers (notably ^{135}Xe and ^{149}Sm). The thorium-based mixed oxide fuel (Th-^{233}U-^{235}U)O_2 exhibits higher reactivity than UO_2 (Table 5). For the solid-pin reference, the k_{inf} (no-leakage multiplication factor) increases from $k_{inf, BOC}$=1.39840 at the beginning of cycle (BOC) for UO_2 to 1.43354 for (Th-^{233}U-^{235}U)O_2, and (Th-^{233}U-^{235}U)O_2 maintains $k_{inf, EOC} \approx$ 1.002-1.004 at the end of cycle (EOC), whereas UO_2 drops below unity ($k_{inf, EOC}$=0.96818). This advantage is attributed to the dual-fissile content (^{233}U and ^{235}U), where ^{233}U provides better thermal-spectrum neutron economy through a higher reproduction factor, η (neutrons produced per absorption in fuel), than ^{235}U alone (2.29 for ^{233}U vs. 2.07 for ^{235}U). In the annular sweep, increasing the inner moderator radius reduces $k_{inf,\,BOC}$ (1.45825 to 1.40666) due to stronger neutron streaming/leakage and modified self-shielding, yet $(Th\text{-}^{233}U\text{-}^{235}U)O_2$ fuel remains comparatively stable, achieving ~166-174 GWd/t discharge burnup under a three-batch refueling strategy, versus 142.44 GWd/t for solid UO_2 (Table 5).

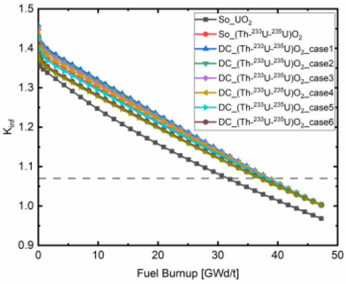

Fig. 3. Variation of k_{inf} with burnup for the investigated cases.

Table 5. k_{inf} at BOC and EOC, cycle burnup and discharge burnup for a 3-batch refueling scheme.

	k_{inf} (BOC)	k_{inf} (EOC)	Cycle burnup (GWd/t)	Discharge burnup (GWd/t)
So_UO_2	1.39840	0.96818	47.48	142.44
So_$(Th\text{-}^{233}U\text{-}^{235}U)O_2$	1.43354	1.00385	56.93	170.80
DC_$(Th\text{-}^{233}U\text{-}^{235}U)O_2$_case1	1.45825	1.00244	57.85	173.54
DC_$(Th\text{-}^{233}U\text{-}^{235}U)O_2$_case2	1.45375	1.00269	57.71	173.12
DC_$(Th\text{-}^{233}U\text{-}^{235}U)O_2$_case3	1.44787	1.00301	57.52	172.57
DC_$(Th\text{-}^{233}U\text{-}^{235}U)O_2$_case4	1.44130	1.00328	57.29	171.88
DC_$(Th\text{-}^{233}U\text{-}^{235}U)O_2$_case5	1.42674	1.00334	56.66	169.98
DC_$(Th\text{-}^{233}U\text{-}^{235}U)O_2$_case6	1.41141	1.00231	55.76	167.29
DC_$(Th\text{-}^{233}U\text{-}^{235}U)O_2$_case7	1.40666	1.00178	55.43	166.30

The radial PPF is defined as the ratio of the maximum pin power to the average assembly pin power, and it is a key indicator for thermal margin and fuel integrity. For Westinghouse-type PWR operation, a commonly adopted design limit is PPF ≤ 1.65, ensuring sufficient margin to DNBR and cladding temperature constraints [16,25]. Figure 4 shows that the hot pins (red-marked locations) remain highly localized and that all configurations exhibit well-flattened power maps. In particular, the thorium-based fuel provides the most uniform distributions: the solid $(Th\text{-}^{233}U\text{-}^{235}U)O_2$ case reaches a maximum PPF of 1.055 at BOC, decreasing to 1.043 at EOC, while the annular thorium cases remain similarly low with a maximum hotspot of about 1.056. These values are far below the 1.65 guideline, corresponding to an approximate 36% margin to the recommended limit, confirming that the proposed lattices maintain comfortable radial peaking margins across burnup.

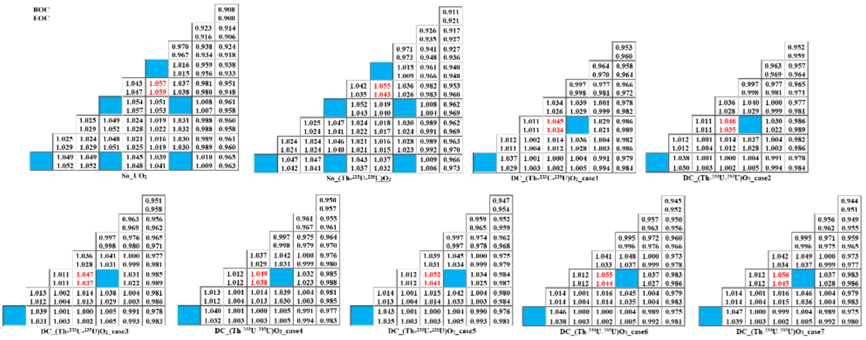

Fig. 4. Pin power distribution with 1/8 assembly symmetry for the investigated cases.

Reactivity feedbacks were quantified using the FTC and MTC, which are key indicators of inherent stability and safety under temperature perturbations. As summarized in Table 6, all cases exhibit negative FTC and MTC, confirming that temperature increases introduce negative reactivity feedback. The FTC magnitude becomes more negative as the inner moderator radius increases in the annular designs, evolving from about -1.69 to -2.32 pcm/K for the thorium annular cases, while the solid fuels yield -1.72 pcm/K (UO_2) and -2.01 pcm/K (Th-^{233}U-^{235}U)O_2. In contrast, the MTC is strongly negative for UO_2 (-39.58 pcm/K for the solid case), whereas thorium-based lattices show less negative MTC for small inner radii (≈ -14 to -23 pcm/K) but trend toward more negative values at larger inner radii (down to -34.77 pcm/K). Overall, enlarging the inner moderator region strengthens temperature feedbacks, particularly for the thorium configurations, thereby improving controllability and thermal-safety margins.

Table 6. Comparison of the FTC and MTC for the investigated cases.

	FTC [pcm/K]	MTC [pcm/K]
So_UO_2	-1.72	-39.58
So_(Th-^{233}U-^{235}U)O_2	-2.01	-20.90
DC_(Th-^{233}U-^{235}U)O_2_case1	-1.69	-14.25
DC_(Th-^{233}U-^{235}U)O_2_case2	-1.75	-14.42
DC_(Th-^{233}U-^{235}U)O_2_case3	-1.82	-16.25
DC_(Th-^{233}U-^{235}U)O_2_case4	-1.91	-17.49
DC_(Th-^{233}U-^{235}U)O_2_case5	-2.09	-19.79
DC_(Th-^{233}U-^{235}U)O_2_case6	-2.27	-22.82
DC_(Th-^{233}U-^{235}U)O_2_case7	-2.32	-34.77

3.2 Thermal-hydraulic results

Figure 5 summarizes the axial evolution of coolant temperature and DNBR for all investigated channels. Starting from the same inlet condition (~562 K), the coolant temperature increases smoothly along the core, reaching outlet values around 597-598 K, with only minor differences among solid and annular cases; the thorium-based configurations show a slightly higher outlet temperature (up to ~0.8 K), indicating marginally larger heat addition. Importantly, the temperature curves remain monotonic and well-behaved, suggesting stable single-phase heat transfer without localized anomalies. The DNBR profiles exhibit the expected U-shaped trend: high values at the inlet (~12), a minimum near mid-height where heat flux is largest, and partial recovery toward the outlet. For all cases, the minimum DNBR is approximately 2.3, which remains comfortably above typical PWR design limits (~1.3-1.5). Variations with inner moderator radius are very small, and the curves nearly overlap, indicating that the neutronic optimization of the inner channel does not penalize thermal-hydraulic safety margins. Overall, thorium-based annular designs maintain robust DNBR margins while preserving comparable coolant heating characteristics.

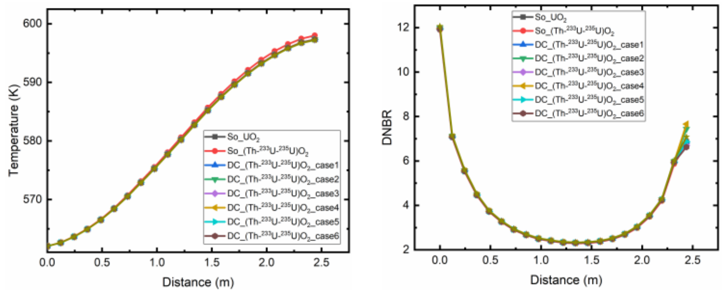

Fig. 5. Temperature and DNBR values for the investigated cases.

4 Conclusions

This work assessed a dual-cooled annular fuel concept for SMR conditions using coupled lattice neutronics and hot-channel thermal–hydraulics while varying the inner moderator radius. The thorium-based $(Th\text{-}^{233}U\text{-}^{235}U)O_2$ fuel outperformed UO_2, reaching 166.3-173.5 GWd/t discharge burnup (three-batch) versus 142.4 GWd/t for solid UO_2. Power distributions remained well flattened (PPF ≈ 1.056, well below the 1.65 guideline). All cases showed negative FTC and MTC, with larger inner radii generally strengthening negative feedback. Thermal-hydraulic behavior was stable and weakly sensitive to geometry, with similar outlet temperatures (~597-598 K) and robust DNB margin (minimum DNBR ~ 2.3).

References

1. M. S. Kazimi and P. Hejzlar, *High Performance Fuel Design for Next Generation PWRs: Final Report* (2006)
2. P. Hejzlar and M. S. Kazimi, Nucl. Technol. **160**, 2 (2007)
3. D. Feng, P. Hejzlar, and M. S. Kazimi, Nucl. Technol. **160**, 16 (2007)
4. M. S. Kazimi, Nucl. Technol. **160**, 1 (2007)
5. Y. S. YANG, C. H. SHIN, T. H. CHUN, and K. W. SONG, J. Nucl. Sci. Technol. **46**, 836 (2009)
6. C. H. Shin, T. H. Chun, D. S. Oh, and W. K. In, Nucl. Eng. Des. **243**, 291 (2012)
7. M. Zaidabadi Nejad and G. R. Ansarifar, Ann. Nucl. Energy **138**, 107185 (2020)
8. M. Z. Nejad and G. R. Ansarifar, Nucl. Eng. Des. **360**, 110518 (2020)
9. Z. Zhang, T. Wu, Y. Wang, S. Chen, C. Yuan, and J. Zhu, Nucl. Mater. Energy **29**, 101068 (2021)
10. S. Uzun, Y. Genç, H. Rifai, O. Kabach, B. Uzun, Z. Sadoune, E. M. Chakir, H. Amsil, and F. El Banni, Nucl. Energy Technol. **11**, 231 (2025)
11. H. Rifai, O. Kabach, Z. Sadoune, E. M. Chakir, S. Uzun, H. Amsil, and F. El Banni, Nucl. Eng. Des. **442**, 114274 (2025)
12. F. El Banni, B. L. H. Gogon, O. Kabach, and E. M. Chakir, Nucl. Energy Technol. **10**, 169 (2024)
13. IAEA, *SMALL MODULAR REACTOR TECHNOLOGY CATALOGUE* (2024)
14. Westinghouse Electric Company LLC, (2023)

15. G. Marleau, A. Hebert, R. Roy, and A. Hébert, *A USER GUIDE FOR DRAGON VERSION5* (2021)
16. O. El Kheiri, O. Kabach, and A. Chetaine, Prog. Nucl. Energy **160**, 104680 (2023)
17. M. J. Driscoll, T. J. Downar, and E. E. Pilat, *The Linear Reactivity Model For Nuclear Fuel Management* (American Nuclear Society, 1991)
18. R. Hernandez and N. R. Brown, Ann. Nucl. Energy **144**, 107555 (2020)
19. Zhiwen Xu, Design Strategies for Optimization High Burn-up Fuel in Pressurized Water Reactor Reactors, Massachusetts Institute of Technology, 2003
20. E. D. Kitcher and S. S. Chirayath, Ann. Nucl. Energy **97**, 232 (2016)
21. V. Ghazanfari, M. Talebi, J. Khorsandi, and R. Abdolahi, Prog. Nucl. Energy **91**, 285 (2016)
22. NRC, *Chapter 4.4: Thermal and Hydraulic Design* (2007)
23. L. . Tong and Y. . Tang, *Boiling Heat Transfer and Two-Phase* (1997)
24. B. S. Shiralkar, E. E. Polomik, R. T. Lahey, J. M. Gonzales, D. W. Radcliffe, and L. E. Schnebly, *Transient Critical Heat Flux—Experimental Results. General Electric Report, GEAP 13295* (1972)
25. A. Erfaninia, A. Hedayat, and S. M. Mirvakili, Prog. Nucl. Energy **93**, 218 (2016)